


Mehdi Jafari Vardanjani,¹ Jacek Senkara ²

A theoretical analysis of vibrational stress relief in AISI 1008 as a mechanical treatment

Vibrational stress relief (VSR) treatment as a method of stress relief is currently performed on different alloys and sizes as an appropriate alternative for thermal stress relief (TSR) method. Although many studies have been performed to extend the knowledge about this process, analytical studies in the field of VSR process seems to require wider efforts to introduce the concept more clearly and extensively. In this study, a theoretical model is proposed based on an analytical equation. The proposed equation was modified in terms of required variables including frequency, amplitude, and vibration duration to encompass more practical parameters compared to the previous models. Thus, essential VSR parameters including the number of cycles as a representative of treatment duration, strain rate as a representative of frequency, and the amplitude were embedded in the model to make it comprehensively practical. Experimental tests were also performed and residual stress distribution was measured by X-ray diffractometry (XRD) method for certain points to compare the experimental results with the theoretical output. An acceptable range of conformation was observed between theoretical and experimental results.

1. Introduction

For a long time, alternative techniques of stress relief such as vibratory techniques have been used in manufactured products to decrease residual stresses. The common method used in big cast or welded components for stress relief has also been aging. Recent studies have shown that vibratory techniques accelerate the process. The scientists claim that regulated vibration provides as much stress

✉ Mehdi Jafari Vardanjani, e-mail: m-jafari@tvu.ac.ir

¹Department of Mechanical Engineering, Technical and Vocational University (TVU), Tehran, Iran.

²Department of Welding Engineering, Warsaw University of Technology, Poland. ORCID: 0000-0001-8082-8307.



© 2021. The Author(s). This is an open-access article distributed under the terms of the Creative Commons Attribution-NonCommercial-NoDerivatives License (CC BY-NC-ND 4.0, <https://creativecommons.org/licenses/by-nc-nd/4.0/>), which permits use, distribution, and reproduction in any medium, provided that the Article is properly cited, the use is non-commercial, and no modifications or adaptations are made.

relief as it can be obtained in months or years in a natural aging process [1]. The study results demonstrated by McGoldrick [2] and Sedak [3] in weldments have proven that vibratory treatment in resonant mode can provide some dimensional accuracy. The weldments have been successfully tested under working conditions.

Lokshin [4] was able to reduce stress relief up to 70% in cast aluminum components using vibratory stress relief (VSR) and stress redistribution. Moore [5] tested a tapered cantilever beam under cyclic loading and showed that stress relief to some degrees could be accomplished.

The VSR efficiency was evaluated on thick aluminum sheets in various research [6, 7]. In these research it is claimed that the VSR also has some influences on the stress concentration that affects material hardness and rigidity. In another study, Khan et al. [8] investigated microhardness as a criterion for detecting the effect of VSR treatment in various areas such as heat-affected zone (HAZ), base metal, and weld bead. While it is not proven that microhardness is a guaranteed parameter to imply residual stress extent, it can be used as a useful indirect criterion to check the proportion of stress reduction.

Wang et al. [9] verified stress relief in the alloy Al-Mg-Si-Cu and found that cyclic force can influence microstructure. Higher vibration rates, as cited by He et al., can also be effective in altering mechanical characteristics [10]. Besides frequency, amplitude, and treatment time in the VSR, Wang et al. also verified the load waveform influence the stress relief process in an experiment [11]. Although the use of sinusoidal waves in vibrations is common, the author claims that a different waveform, such as the Wavelet (an innovative waveform introduced in this research), can be even more efficient in reducing residual stresses.

The impact of ultrasonic vibration was also investigated on the mechanical characteristics and microstructure of a hyper-eutectic aluminum alloy by Lin [12], and the results showed that the average grain size can be reduced to approximately 21~24 μm by the VSR.

There are also studies that bring a broader contribution to analytical and theoretical aspects of the VSR process in addition to numerical solutions provided for stress relief mechanism analysis [13, 14]. For instance, Kwofie [15] proposed a model of plasticity to simulate and describe the VSR phenomenon. The model is based on the assumption that cyclic stresses are induced by internal vibratory forces that combine with the remaining stresses in the material. Residual stress relief therefore happens when the amount of the induced cyclic stress and the residual stress exceeds the material's local yield stress. As the author claims, the impact of loading and material parameters such as vibration frequency, stress amplitude, strain amplitude, yield stress and original strain hardening rate can be explained or analyzed in the light of this model. Although the model is well-worked on and different parameters are included, practical verification of the model has not been provided in the study and the complexity of the equation requires extra calculation efforts to obtain the remaining residual stress value as an output.

Aoki et al. [16] also proposed a modern method for reduction of residual stress by harmonic vibrational loading during welding. The proposed method was tested experimentally while residual stress was measured by X-ray diffractometry (XRD). In addition, an analytical method involving mass and preloaded springs with elasto-plastic properties was used to demonstrate the reduction of residual stress. The model is straightforward enough for the process in which the effect of frequency and amplitude can be monitored, however, there are some doubt about the representation of elasto-plastic properties by the springs. In addition, the effect of the number of the cycles cannot be directly however, the model is well-designed and verified experimentally.

Rao et al. [17] examined cyclic stress and strain of welded 304L stainless steel parts and a mathematical model of residual stress relief was proposed for dynamic stress evaluation. The model was applied to consider the influence of the VSR during manufacturing welded structures. As the author claims, the difference between the calculated and measured residual stress reduction has been about 11%. The model is developed mostly by using empirical data and subtle theoretical modifications can be seen, in addition to the simplicity of the model.

Wang et al. [18] also used an ARM microprocessor and frequency spectrum analysis in their study for hardware architecture in the VSR process. As the authors claim, it reduces the size and cost of the system for performing the VSR. The nature of the study is rather experimental than analytical as it focuses more on the simplification of the VSR treatment hardware by using compact-size microprocessor and frequency spectrum analysis while only a few theoretical equations can be found within the study. In Dawson's research [1] it is stated that VSR methods provide tremendous surface stress relaxation in rolled mild steel and certain aluminum alloys due to plastic deformations.

The analytical method described in this study is based on the traditional plasticity with linear kinematic hardening and it demonstrates some of the insufficiently investigated theoretical aspects of the process. The equation known from the Dawson's study was used as a basic form of the proposed model in the current study, and it was adequately modified according to the required parameters which have rarely been included in the theoretical VSR models. Analytical aspects of the VSR method were analyzed to calculate residual stress distribution after the VSR. Therefore, Dawson's equation [1] was modified to account for the effect of frequency and time of VSR, while in the previous formulation only loading had been included as the main variable of the VSR. Amplitude of the vibration is also considered as a direct parameter in the equation instead of the moment or the loading variable. Experimental phase of the research is performed according to a similar previous study [19] to check the effect of frequency, time, and amplitude, while the derived equations are used to check the same conditions as in the experimental tests. Experimental results were also used to check the validity of results, and the observed discrepancies were acceptable.

2. Methods and materials

2.1. Experiments

The material AISI 1008 was chosen to be analyzed experimentally and theoretically for the purpose of verifying the proposed VSR equational model. Table 1 lists important mechanical properties of AISI 1008. The experiments are performed in three steps, as follows.

Table 1.

Mechanical Properties of AISI 1008

Parameter	Value
E (Young modulus) (GPa)	200
E_T (Slope of simplified stress-strain diagram in plastic zone) (GPa)	8
S_y (Yield strength) (MPa)	250
S_{ut} (Ultimate tensile strength) (MPa)	350
ρ (Density) (Kg/m ³)	7800
ν (Poison ratio)	0.3

2.1.1. Imposing the initial stress distribution by applying the moment

Initial residual stresses can be imposed by different operations during any manufacturing processes such as machining, welding, etc. In this study, it is essential to impose the residual stresses by applying an external moment, to be in accordance with the theoretical method. Therefore, the initial residual stresses were imposed by applying a force with the same value as that defined in the theoretical analysis. It should be mentioned that applying an initial stress gradient caused by the welding process was also considered, as in other studies in the field of spot welding [20, 21]. However, it was concluded that external loading would yield a more appropriate distribution for the current study. The configuration of the loading is the same as the one used in the VSR process (Fig. 1). The required deflection of the beam tip is calculated using Eq. (11) and (17), which will be explained in detail in the next sections.

Although there is a deflection after applying the first loading due to plastic deformations taking place in the layers of beam section, it does not hinder performing the VSR process in the next steps. The reason is that this deflection is not large enough to deteriorate the VSR setup. Furthermore, the VSR process can be performed on the deformed beam if the amplitude of the vibration is set appropriately. In addition, the VSR is performed in 2 steps to keep a permanent contact between the tool and specimen during the experiment, which will be explained more precisely in the next section.

2.1.2. VSR

The schematics of the VSR setup is shown in Fig. 1 and Fig. 2. Fig. 3 demonstrates the beam under VSR treatment. Here, we have chosen the VSR setup used in the previous study [19], in which a lathe machine is considered to be the source of vibration while the tool holder clamps the specimen. Nevertheless, there are modifications introduced, such as a more controllable lathe machine and a specific crank shaft as the eccentric tool in the chuck for applying certain vibration

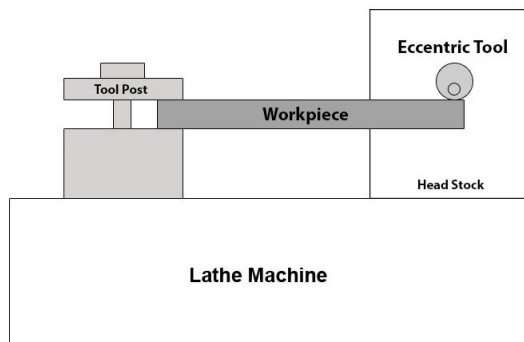


Fig. 1. VSR configuration

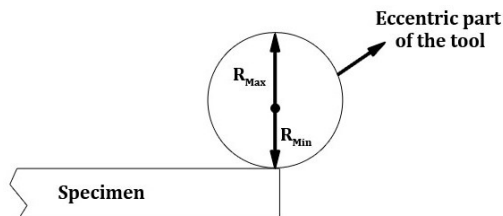


Fig. 2. Initial position of tool and specimen to keep contact with eccentric part of the tool at each step

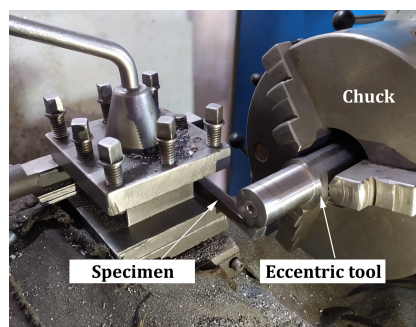


Fig. 3. VSR treatment being performed on sample using eccentric tool clamped in the spindle

amplitudes (Fig. 4). The frequency is adjusted by setting the spindle speed as each turn of the spindle corresponds to one cycle of the VSR treatment. The tool and the specimen are set in contact at the ending part of the specimen during the VSR treatment by rotational positioning of the eccentric tool in such a way that initially it contacts the specimen at the point with minimum radius of the eccentric tool (Fig. 2). Therefore, the contact between the tool and the specimen is permanently maintained, since the remaining points of the perimeter push the specimen down creating the bending moment for the VSR process during each rotation. It should be noted that, when there are plastic deformations in the specimen, the contact might be lost because the part bends and loses its initial shape. In addition, the VSR process should be carried out in opposite directions to be more effective and also be consistent with the assumptions of the theoretical section. This issue was resolved by performing the VSR process in two steps to apply a fully reversible loading on the specimen. In the first step, the specimen is treated during the full number of cycles on the part. Then, in the second step, the VSR treatment is repeated while the treated part is rotated by 180° .



Fig. 4. Eccentric AISI 4340 tools for applying loads with certain amplitudes

Although natural frequency was not considered as the main parameter during the analysis, it was estimated using an accelerometer, an instrumented hammer, and a Fast Fourier Transform (FFT) vibration analyzer [22, 23] in order to assure the VSR configuration and the process correctness, with regard to the applied frequency. The natural frequency was also checked in the finite element model using the same method as that performed by Yang [14].

2.1.3. Residual stress measurement

Residual stress measurement was performed using the low-angle XRD method before and after the VSR process. This measurement was performed in different points on the cross section of the cut samples and the ending face. Since there are

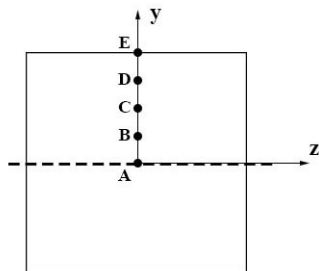
usually some extra residual stresses added due to the cutting process, the first ones have been compared to the values obtained from the ending face, and observed discrepancies were acceptable.

The device specifications is listed in Table 2. Residual stresses were obtained in several points on the section after cutting samples into smaller parts, as indicated in Fig. 5.

Table 2.

Technical specifications of XRD low angle device used to measure residual stresses

Parameter	Value
Configurations	θ/θ or $\theta/2\theta$
Measuring diameter	500 mm and 560 mm
Angular range	360°
Max. usable angular range	$-110^\circ < 2\theta \leq 168^\circ$
Smallest addressable increment	0.0001°



(a)



(b)

Fig. 5. (a) Residual stress measurement points (A to E) on specimen cross section; (b) A cut sample for XRD measurement

2.2. Theoretical method

The residual stress distribution before the VSR treatment is described in the previous study [19]. Assuming that the whole stress applied remains in the part in the worst case, it can be calculated as below:

$$\sigma_i = \left(\frac{y}{c - h_1} \right) \sigma_e, \quad 0 \leq y \leq c - h_1, \quad (1)$$

$$\sigma_i = \left(1 - \beta + \frac{\beta y}{c - h_1} \right) \sigma_e, \quad c - h_1 \leq y \leq c, \quad (2)$$

where σ_i is the initial residual stress distribution at the initial stage before performing any stress relief treatment; this is the condition of the part after the manufact-

turing process. σ_e is the yield strength of the material, I is moment of inertia, c is the half of the height of the beam section, and h_1 is the half of the height of the beam section in which plastic deformation takes place at the initial conditions of the part. As mentioned in the previous study [19], β is defined according to the following equation:

$$\beta = \frac{E_T}{E}. \quad (3)$$

It should be noted that σ_e is assumed to appear after applying the initial moment M_0 , where:

$$\sigma_e = \frac{M_0 y_0}{I}, \quad (4)$$

where:

$$y_0 = c - h_1. \quad (5)$$

Then, the stress distribution after 2 cycles of VSR can be calculated as follows:

$$\sigma_{ir} = \left(\frac{y}{c - h_1} \right) \sigma_e - \frac{M_1 y}{I}, \quad 0 \leq y \leq c - h_1, \quad (6)$$

$$\sigma_{ir} = \left(1 - \beta + \frac{\beta y}{c - h_1} \right) \sigma_e - \frac{M_1 y}{I}, \quad c - h_1 \leq y \leq c, \quad (7)$$

$$\sigma_{fr} = \left(\frac{1}{c - h_1} - \frac{2}{c - h_2} \right) y \sigma_e + \frac{M_2 y}{I}, \quad 0 \leq y \leq c - h_1, \quad (8)$$

$$\sigma_{fr} = \left(1 - \beta + \frac{\beta y}{c - h_1} - \frac{2y}{c - h_2} \right) \sigma_e + \frac{M_2 y}{I}, \quad c - h_1 \leq y \leq c - h_2, \quad (9)$$

$$\sigma_{fr} = \left(-1 + \beta + \frac{\beta y}{c - h_1} - \frac{2\beta y}{c - h_2} \right) \sigma_e + \frac{M_2 y}{I}, \quad c - h_2 \leq y \leq c, \quad (10)$$

where σ_{ir} is the residual stress distribution at the initial stage while applying first bending moment (M_1) in VSR (Fig. 6), σ_{fr} is the residual stress distribution while applying the second bending moment (M_2) in opposite direction (Fig. 7), and h_2 is the half of the height of the beam section at which plastic deformation takes place at the second moment.

On inspection of Eq. (8) through (10), we can deduce that only loading (moment) has been considered for calculating the value of the relieved stress and nothing has been mentioned about frequency, time, and amplitude. These parameters are considered to be introduced into the equations, as follows.

Since the configuration of the beam is the same as that of a cantilever beam, and the applied load is a perpendicular force at the end of the beam, the maximum bending stress equation $\left(M_e = \frac{\sigma_e I}{c} \right)$ takes the form:

$$P_e = \frac{\sigma_e I}{cL}, \quad (11)$$

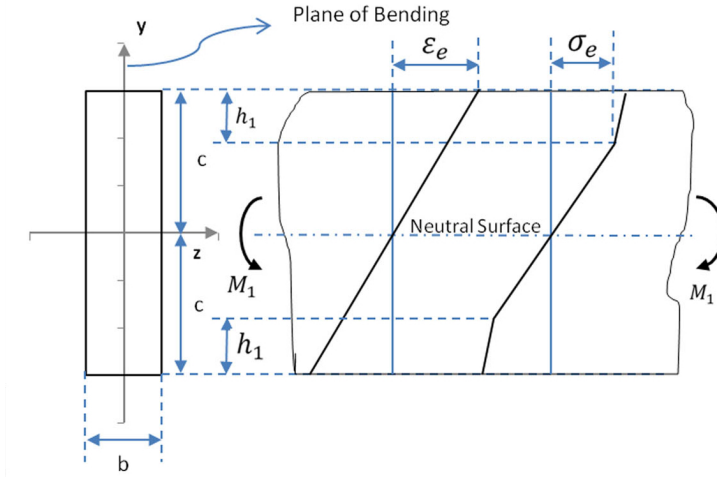


Fig. 6. Stress distribution while M_1 is applied [19]

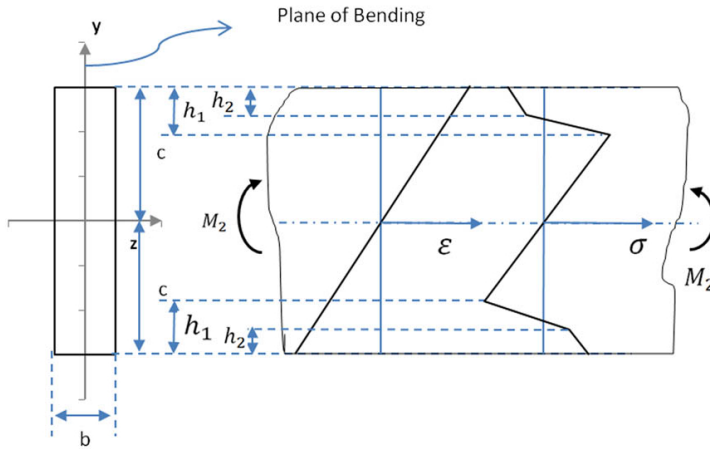


Fig. 7. Stress distribution while M_2 is applied [19]

where P_e is the maximum force before yielding of the fixed end, and L is the length of the beam. Accordingly, Eq. (1) through (10) can be modified as follows:

$$\sigma_{ir} = \left(\frac{y}{c - h_1} \right) \sigma_e - \frac{P_1 L y}{I}, \quad 0 \leq y \leq c - h_1, \quad (12)$$

$$\sigma_{ir} = \left(1 - \beta + \frac{\beta y}{c - h_1} \right) \sigma_e - \frac{P_1 L y}{I}, \quad c - h_1 \leq y \leq c, \quad (13)$$

$$\sigma_{fr} = \left(\frac{1}{c - h_1} - \frac{2}{c - h_2} \right) y \sigma_e + \frac{P_2 L y}{I}, \quad 0 \leq y \leq c - h_1, \quad (14)$$

$$\sigma_{fr} = \left(1 - \beta + \frac{\beta y}{c - h_1} - \frac{2y}{c - h_2}\right) \sigma_e + \frac{P_2 Ly}{I}, \quad c - h_1 \leq y \leq c - h_2, \quad (15)$$

$$\sigma_{fr} = \left(-1 + \beta + \frac{\beta y}{c - h_1} - \frac{2\beta y}{c - h_2}\right) \sigma_e + \frac{P_2 Ly}{I}, \quad c - h_2 \leq y \leq c. \quad (16)$$

It is assumed that the VSR is performed in opposite directions in each period (a certain number of cycles), therefore the signs in equations don't changed compared to Eq. (8) to (10) in which the moments are reversed. The maximum deflection at the free end of the beam (δ) can be expressed by:

$$\delta = \frac{PL^3}{3EI}, \quad (17)$$

$$\Rightarrow P = \frac{3\delta EI}{L^3}. \quad (18)$$

Thus, Eq. (14) through (16) can be modified to the following form:

$$\sigma_{fr} = \left(\frac{1}{c - h_1} - \frac{2}{c - h_2}\right) y \sigma_e + \frac{3\delta EI}{L^3} Ly, \quad 0 \leq y \leq c - h_1, \quad (19)$$

$$\sigma_{fr} = \left(1 - \beta + \frac{\beta y}{c - h_1} - \frac{2y}{c - h_2}\right) \sigma_e + \frac{3\delta EI}{L^3} Ly, \quad c - h_1 \leq y \leq c - h_2, \quad (20)$$

$$\sigma_{fr} = \left(-1 + \beta + \frac{\beta y}{c - h_1} - \frac{2\beta y}{c - h_2}\right) \sigma_e + \frac{3\delta EI}{L^3} Ly, \quad c - h_2 \leq y \leq c. \quad (21)$$

However, there are still no terms representing frequency and time. Therefore, these equations (Eq. (19) to (21)) are planned for calculating stress relief taking place only at the first cycle. By adding n as the number of applied cycles, following equations will be derived:

$$\sigma_{fr} = \left(\sum_{i=1}^n \frac{(-1)^{i+1} i}{c - h_i}\right) y \sigma_e + \frac{3\delta_n E}{L^2} y, \quad 0 \leq y \leq c - h_1, \quad (22)$$

$$\sigma_{fr} = \left(1 - \beta + \sum_{i=1}^n \frac{\beta \frac{(-1)^{i+1} + 1}{2} (-1)^{i+1} i y}{c - h_i}\right) \sigma_e + \frac{3\delta_n E}{L^2} y, \quad (23)$$

$$c - h_i \leq y \leq c - h_{i+1} \quad (i = 1, \dots, n-1),$$

$$\sigma_{fr} = \left(-1 + \beta + \beta y \sum_{i=1}^n \frac{(-1)^{i+1} i}{c - h_i}\right) \sigma_e + \frac{3\delta_n E}{L^2} y, \quad c - h_n \leq y \leq c. \quad (24)$$

Therefore, the effect of time is also accounted for in the equation; and h_i is calculated by accounting for the previous moment applied. Before going further with the equations, it must be noted that all the equations derived above are based on different moments applied on the beam. However, identical moments are assumed at each cycle of the VSR, since the amplitudes don't change during the treatment. This assumption changes the equation structure as h_i is equal during the whole process, since h value is calculated based on the applied moment. By assuming the same h for each cycle, Eq. (22) to (24) are reduced to the following forms:

$$\sigma_{fr} = \left(\sum_{i=1}^n \frac{(-1)^{i+1} i}{c-h} \right) y \sigma_e + \frac{3\delta_n E}{L^2} y, \quad 0 \leq y \leq c-h, \quad (25)$$

$$\sigma_{fr} = \left(-1 + \beta + \beta y \sum_{i=1}^n \frac{(-1)^{i+1} i}{c-h} \right) \sigma_e + \frac{3\delta_n E}{L^2} y, \quad c-h \leq y \leq c. \quad (26)$$

The value of h can be calculated based on the amplitude of the vibration (δ_n). According to Eq. (4) and (5), h can be calculated as follows:

$$h = c - \frac{\sigma_e I}{M}, \quad (27)$$

$$\Rightarrow h = c - \frac{\sigma_e I}{PL}, \quad (28)$$

$$\Rightarrow h = c - \frac{\sigma_e L^2}{3\delta_n E}. \quad (29)$$

By substituting h into Eq. (25) and (26), these equations take the following forms:

$$\sigma_{fr} = 3 \left(\sum_{i=1}^n \frac{(-1)^{i+1} i \delta_n E}{L^2} \right) y + \frac{3\delta_n E}{L^2} y, \quad 0 \leq y \leq c-h, \quad (30)$$

$$\sigma_{fr} = \sigma_e (\beta - 1) + 3\beta y \sum_{i=1}^n \frac{(-1)^{i+1} i \delta_n E}{L^2} + \frac{3\delta_n E}{L^2} y, \quad c-h \leq y \leq c. \quad (31)$$

As we account for strain rate in the equations, the effect of frequency will appear in the equation. As reported in the study by Li et al. [24], the strain rate influences mechanical properties. The most visible effect of strain rate on steel alloy, described in this study and similar research studies, takes place in the plastic range. In other words, the curvature of the stress-strain diagram changes in the plastic range with the increasing strain rate. Although there is a minor effect on σ_e in very large strain rates, it is ignorable in calculations for the current rates.

Regarding the effect of the strain rate on plastic range, β is directly affected. Thus β' is defined as follows:

$$\beta' = C_{SR}\beta, \quad (32)$$

where C_{SR} is the coefficient of strain rate. According to the study by Li et al. [24], the following equation provides an appropriate approximation of the resulting diagram obtained for different strain rates for steel alloys:

$$C_{SR} = \log_{10} \left[\frac{f}{10} + 1 \right], \quad (33)$$

where f is the frequency of the vibration which represents strain rate in $\frac{1}{s}$ or Hz. Therefore, Eq. (22) through (24) turn into the following form:

$$\sigma_{fr} = 3 \sum_{i=1}^n \frac{(-1)^{i+1} i \delta_n E}{L^2} y + \frac{3 \delta_n E}{L^2} y, \quad 0 \leq y \leq c-h, \quad (34)$$

$$\sigma_{fr} = (\beta - 1) \sigma_e + 3 \beta' y \sum_{i=1}^n \frac{(-1)^{i+1} i \delta_n E}{L^2} + \frac{3 \delta_n E}{L^2} y, \quad c-h \leq y \leq c. \quad (35)$$

As reported in the previous studies, the effect of VSR reduces during the next cycles [1, 25]. This means the calculated stress distribution in Eq. (34) and (35) must be modified according to the number of cycles. After examining different modifications and comparing them with experimental results, it appeared that the averaging method would give the most logical and realistic correction in the following equations:

$$\sigma_{fr} = \frac{3}{n} \sum_{i=1}^n \frac{(-1)^{i+1} i \delta_n E}{L^2} y + \frac{3 \delta_n E}{L^2} y, \quad 0 \leq y \leq c-h, \quad (36)$$

$$\sigma_{fr} = (\beta' - 1) \sigma_e + \frac{3}{n} \beta' y \sum_{i=1}^n \frac{(-1)^{i+1} i \delta_n E}{L^2} + \frac{3 \delta_n E}{L^2} y, \quad c-h \leq y \leq c. \quad (37)$$

It should be noted that Eq. (34) and (35) calculate the stress distribution of the fixed end. This is the critical section of the beam in which the stress values are maximal, and other section are subjected to lower stresses, relative to the distance (x) to the loading point. After some modifications, the following equation is derived with ignorable error, for the whole section:

$$\sigma_{fr} = \frac{3 \delta_n E y}{L^2} \left(\left(\frac{\beta'}{n} \sum_{i=1}^n ((-1)^{i+1} i) \right) \sin \left(\frac{y}{4h} \right) + 1 \right). \quad (38)$$

3. Results and discussion

The calculations are performed according to Table 1 and Table 3 for material and geometric parameters, respectively.

Table 3.

Assumed geometrical values

Parameter	Value
L (m)	0.25
c (m)	0.01

As seen in Fig. 8, the proposed model indicates the effectiveness of the VSR in the first cycles, as reported in the previous studies [1, 19, 25]. Therefore, extending the time of the VSR does not necessarily influence the process unless other parameters, including frequency and amplitude, are increased.

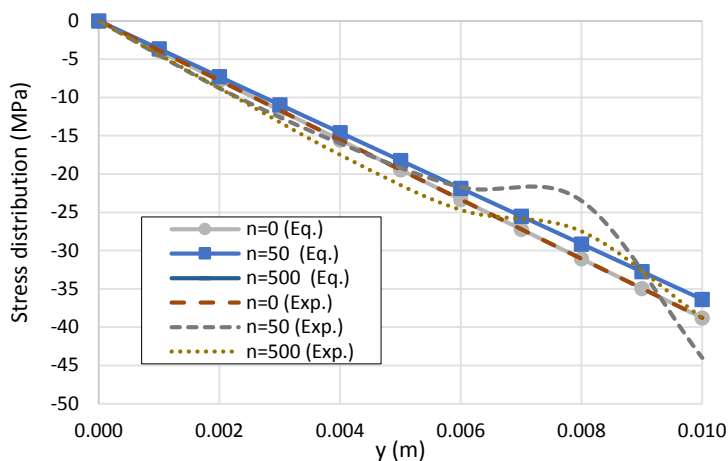


Fig. 8. Stress distribution versus height (y) in section of the beam with $\delta = 1$ mm, $f = 1$ Hz (n is the number of the cycles)

As seen in Fig. 9, residual stress reduction is effectively influenced by frequency, and this effect grows with increasing frequency value, in contrast to the number of cycles (duration or time). Although it is true for the amplitude, the effect of the latter factor is more intense. All these results prove the consistency of the proposed model with experimental results and previous studies.

As seen in Fig. 10, the influence of amplitude is considerable in the first steps of the amplitude values, however, this influence reduces in effect of larger amplitudes. According to Fig. 10, the extent of stress relief diminishes for larger amplitudes and a significant difference is visible between $\delta = 1$ mm and $\delta = 4$ mm. In fact, there should be a limit for the amplitude to be effective in stress-relief process. For

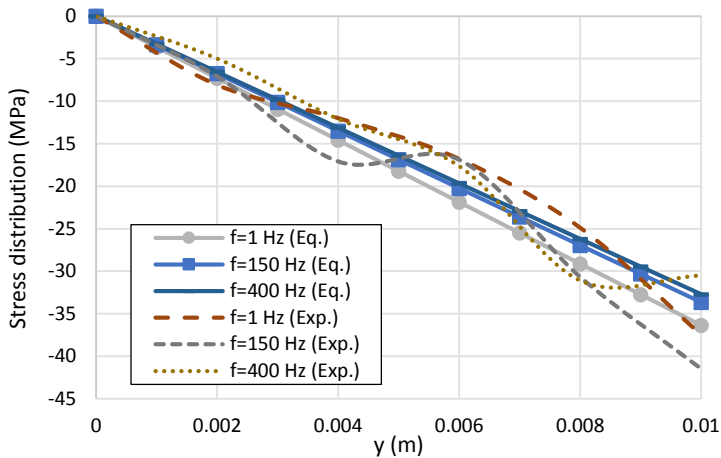


Fig. 9. Stress distribution versus height (y) in section of the beam with $\delta = 1$ mm, $n = 10$ (f is frequency)

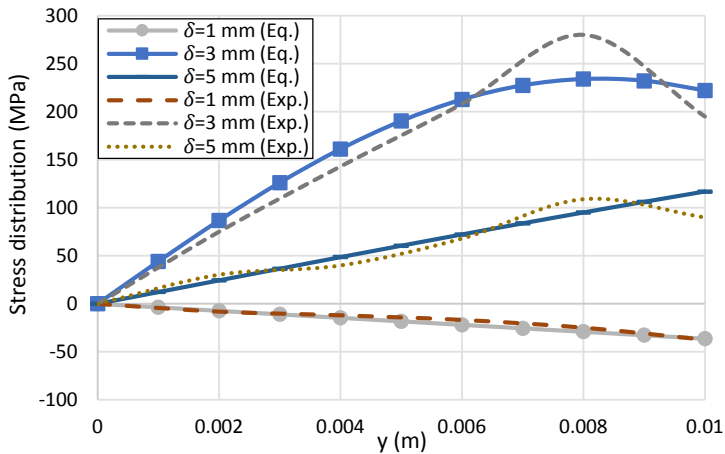


Fig. 10. Stress distribution versus height (y) in section of the beam with $f = 1$ Hz, $n = 10$ (δ is amplitude)

the current study, it converges to $\delta = 5$ mm, or a bit more, maybe to $\delta = 6$ mm, estimated by performing extrapolation.

Fig. 11 to Fig. 13 illustrate the effect of each parameter on the maximum value of predicted residual stress along the y -axis. As seen in Fig. 11 and Fig. 12, the effect of time (number of cycles) and frequency is more visible for the first change and it reduces considerably in the next increment. Furthermore, these two parameters are effective in stress relief for about 3 or 4 MPa. Although this is not a significant effect, it might become larger for the next increments which are not shown in these charts.

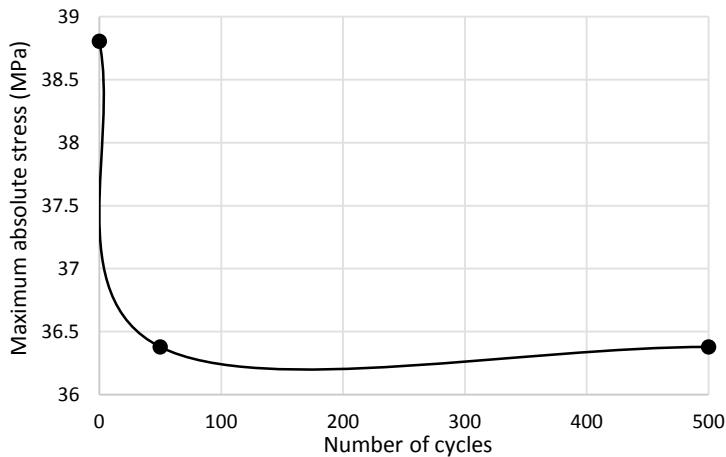


Fig. 11. Maximum absolute value of predicted residual stress along y-axis in beam section with $\delta = 1$ mm, $f = 1$ Hz

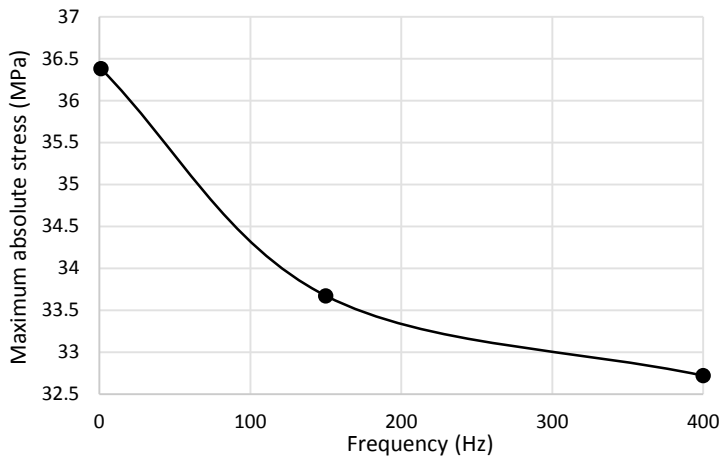


Fig. 12. Maximum absolute value of predicted residual stress along y-axis in beam section with $\delta = 1$ mm, $n = 10$

Although certain ranges of parameters have been chosen to be tested in the experiments, it does not imply the limitation of the proposed analytical model. Larger or smaller values are also possible to be evaluated in the proposed model, while they can be compared to experimental results. For instance, the time variable (number of cycles) might be required to be tested for larger values, however, it is usually predicted to yield to the converged results for longer durations. The effect of vibration frequency can also be examined in other ranges, however, it is also predictable that it converges to a specific value according to the material and other parameters.

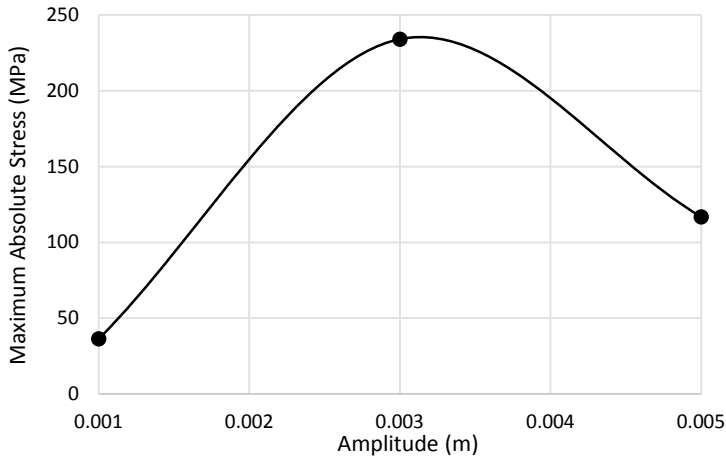


Fig. 13. Maximum absolute value of predicted residual stress along y -axis in beam section with $f = 1$ Hz, $n = 10$

4. Further mathematical analysis

This section is devoted to checking how broadly the proposed model can be used to assure the chosen range of parameters for the VSR process. In other words, other aspects of the model are analyzed by further mathematical considerations to obtain critical domains and range of the equation (function) depending on each effective variable.

To do this, derivatives of the proposed model (Eq. (38)) are calculated and critical points are checked. The following arithmetic simplifications have been assumed before performing the operations, for better understanding of the analysis:

$$\frac{1}{n} \sum_{i=1}^n ((-1)^{i+1} i) \cong \sum_{i=1}^n (2i - 1) - 2 \sum_{i=1}^n i, \quad (39)$$

$$\Rightarrow \frac{1}{n} \sum_{i=1}^n ((-1)^{i+1} i) \cong n^2 - n(n + 1), \quad (40)$$

$$\Rightarrow \frac{1}{n} \sum_{i=1}^n ((-1)^{i+1} i) \cong -n. \quad (41)$$

Thus Eq. (38) will turn to the following form:

$$\Rightarrow \sigma_{fr} \cong \frac{3\delta_n E y}{L^2} \left[-\beta' \sin\left(\frac{y}{4h}\right) + 1 \right]. \quad (42)$$

4.1. Number of cycles

For the first variable to be investigated, the following equation is derived according to Eq. (41):

$$\frac{\partial \sigma_{fr}}{\partial n} = 0. \quad (43)$$

This result is not far from reality, and a similar conclusion has been drawn in previous studies [1, 19, 25], according to which the first cycles constitute the most important part of the VSR process, when a huge fraction of residual stress is removed. In addition, according to Fig. 8, the number of cycles has very low effect on the stress relief process. This fact is graphically depicted in Fig. 11 where it can be seen that, after the first cycle, the number of consecutive cycles has an almost zero effect on reducing the amount of maximum absolute stress.

4.2. Frequency

By using Eq. (3) to (33) and (38), the following form of the equation is derived:

$$\sigma_{fr} = \frac{3\delta_n E y}{L^2} \left(-\frac{E_T}{E} \log_{10} \left(\frac{f}{10} + 1 \right) \sin \left(\frac{y}{4h} \right) + 1 \right), \quad (44)$$

$$\Rightarrow \frac{\partial \sigma_{fr}}{\partial f} = \frac{3 \ln 10 \times \delta_n y E_T}{L^2} \sin \left(\frac{y}{4h} \right) \frac{1}{f + 10}. \quad (45)$$

As shown in Eq. (45), there isn't any critical value for frequency, as this variable appears in the denominator, thus can't reduce the whole equation to zero in the whole domain unless it approaches infinity. However, there are some studies showing that resonant vibrations can introduce a considerable stress relief [26], which does not mean that higher frequencies can't cause a bigger stress relief.

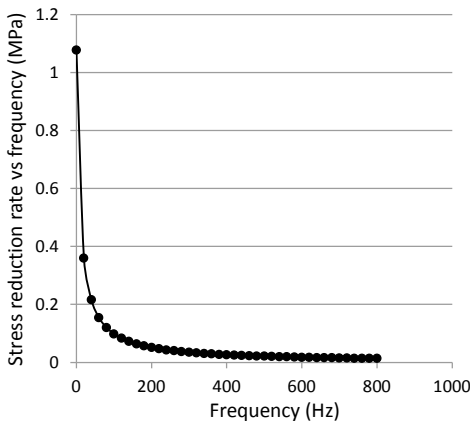


Fig. 14. $\frac{\partial \sigma_{fr}}{\partial f}$ versus f

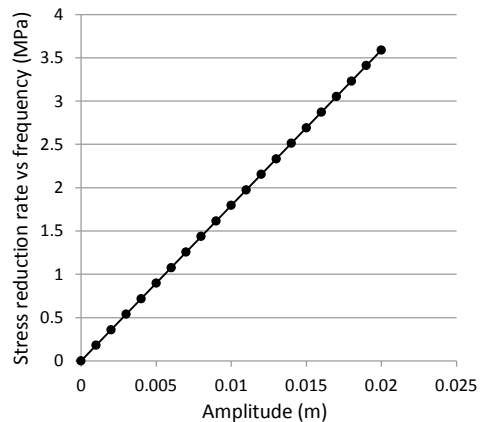


Fig. 15. $\frac{\partial \sigma_{fr}}{\partial \delta_n}$ versus δ_n

In other words, extremely high frequencies should be tested experimentally to test the stress relief capabilities, but it has not yet been done due to practical limitations. Alternatively, it can be performed using ultrasonic vibrations for higher ranges of frequency. By assuming the average values for other variables, Fig. 14 to Fig. 18 are obtained for different variables in Eq. (45). As seen in Fig. 18, there is a linear relationship between E_T and $\frac{\partial \sigma_{fr}}{\partial f}$ according to Eq. (45). Thus, there is a linear ascend in $\frac{\partial \sigma_{fr}}{\partial f}$ by increasing E_T .

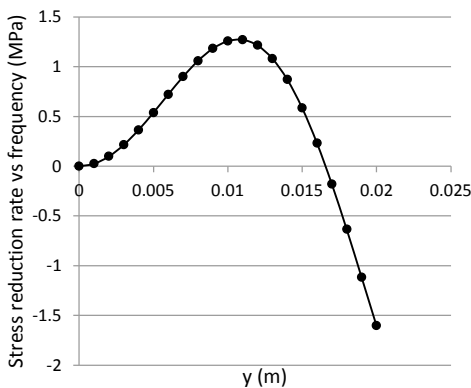


Fig. 16. $\frac{\partial \sigma_{fr}}{\partial f}$ versus y

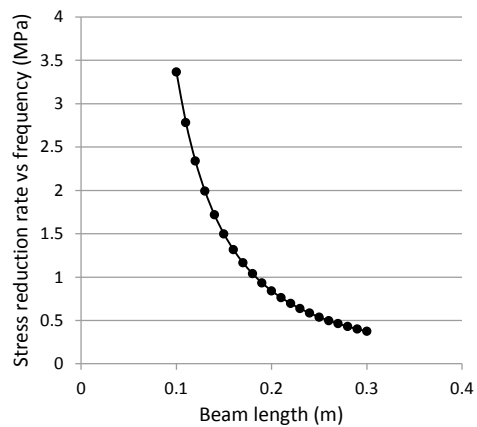


Fig. 17. $\frac{\partial \sigma_{fr}}{\partial f}$ versus L

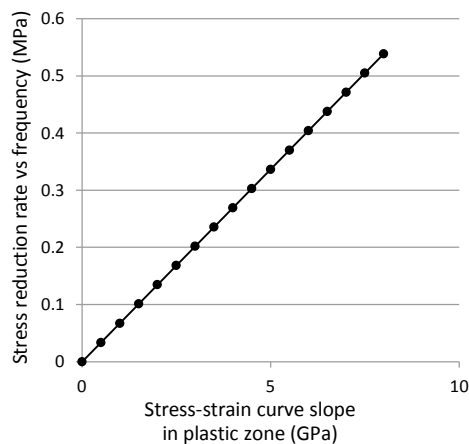


Fig. 18. $\frac{\partial \sigma_{fr}}{\partial f}$ versus E_T

4.3. Amplitude

The following equation is derived according to Eq. (44):

$$\frac{\partial \sigma_{fr}}{\partial \delta_n} = \frac{3y}{L^2} \left[-E_T \log_{10} \left(\frac{f}{10} + 1 \right) \sin \left(\frac{y}{4h} \right) + E \right]. \quad (46)$$

According to Eq. (46), the derivative of the residual stress distribution of δ_n is a constant value. This means that residual stress reduction increases with increasing value of amplitude, unless there are physical limitations such as extensive plastic deformations or flexure. This conclusion is on a par with the obtained diagram in Fig. 10. By assuming the average values for other variables, Fig. 19 to Fig. 23 are

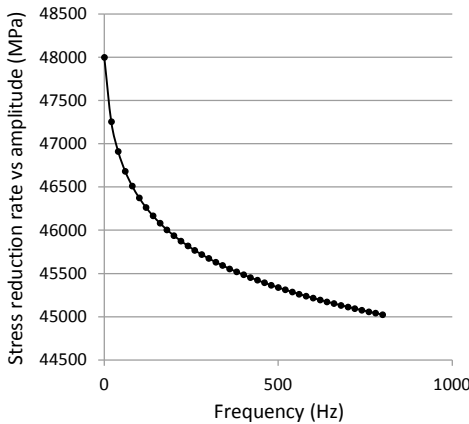


Fig. 19. $\frac{\partial \sigma_{fr}}{\partial \delta_n}$ versus δ_n

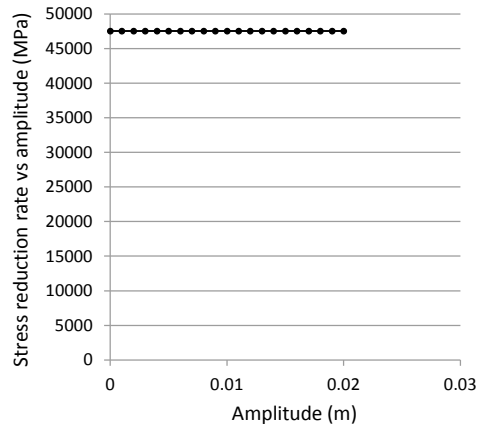


Fig. 20. $\frac{\partial \sigma_{fr}}{\partial \delta_n}$ versus f

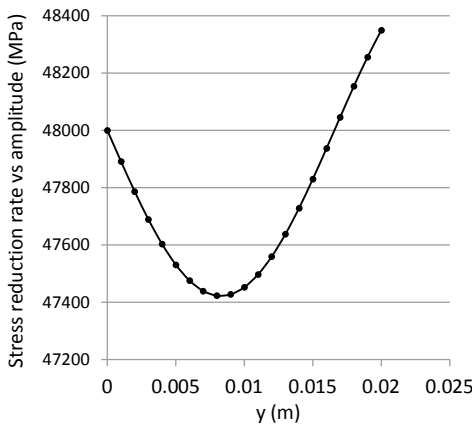


Fig. 21. $\frac{\partial \sigma_{fr}}{\partial \delta_n}$ versus y

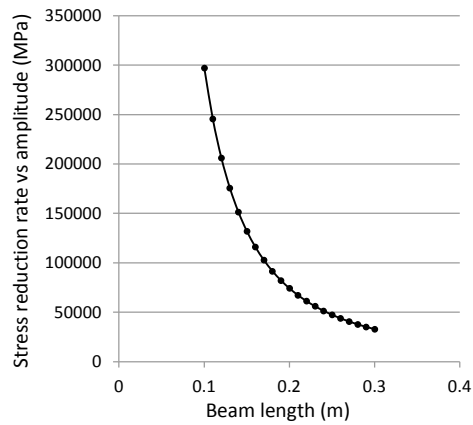


Fig. 22. $\frac{\partial \sigma_{fr}}{\partial \delta_n}$ versus L

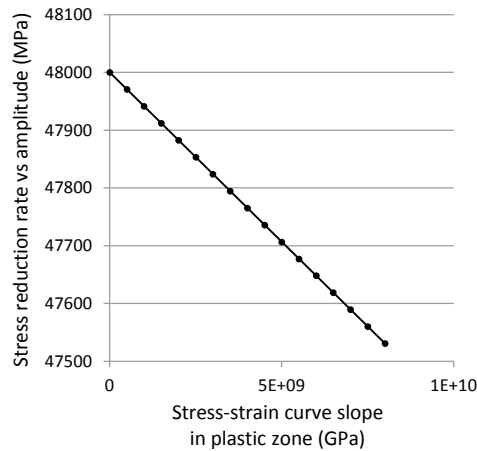


Fig. 23. $\frac{\partial \sigma_{fr}}{\partial \delta_n}$ versus E_T

obtained for different variables in Eq. (46). As seen in Fig. 23, there is a linear relationship between E_T and $\frac{\partial \sigma_{fr}}{\partial \delta_n}$ according to Eq. (46). Thus, there is a linear descend in $\frac{\partial \sigma_{fr}}{\partial \delta_n}$ with increasing E_T .

5. Conclusion

A theoretical modification of the previous model has been proposed for vibrational stress relief process. The aim was to make the model more practical and comprehensive in terms of parameters. The model takes into account the effect of time (number of cycles), load (amplitude), and frequency of the treatment. It is believed that the current model can be used for investigating the effects of parameters on stress relief and for calculating approximate magnitude of the relieved stress. This can be done based on the results and comparison with experiments, on the condition that the configuration of the experiments is as described in the text.

Manuscript received by Editorial Board, April 04, 2021;
 final version, August 11, 2021.

References

- [1] R. Dawson. Residual stress relief by vibration. Ph.D. Thesis, University of Liverpool, UK, 1975.
- [2] R.T. McGoldrick and H.E. Saunders. Experiments in stress-relieving castings and welded structures by vibration. *Journal of the American Society of Naval Engineers*, 55(4):589–609, 1943.

- [3] P. Sędek and M.S. Węglowski. Application of mechanical vibration in the machine building technology. *Key Engineering Materials*, 504-506:1383–1388, 2012. doi: [10.4028/www.scientific.net/kem.504-506.1383](https://doi.org/10.4028/www.scientific.net/kem.504-506.1383).
- [4] I.K. Lokshin. Vibration treatment and dimensional stabilization of castings. *Russian Castings Production*, 10:454–457, 1965.
- [5] H. Moore. A study of residual stresses and size effect and a study of the effect of repeated stresses on residual stresses due to shot peening of two steels. *Proceedings of the Society for Experimental Stress Analysis*, 2(1):170–177, 1944.
- [6] A. Jurcius, A.V. Valiulis, O. Černašėjus, K.J. Kurzydowski, A. Jaskiewicz, and M. Lech-Grega. Influence of vibratory stress relief on residual stresses in weldments and mechanical properties of structural steel joint. *Journal of Vibroengineering*, 12(1):133–141, 2010.
- [7] K. Liao, Y-X. Wu, and J-K. Guo. Application of VSR technique in stress reduction of aluminum alloy thick plate and its limitation. *Journal of Vibration and Shock*, 31(14):70–73, 2012. (in Chinese).
- [8] M.B. Khan and T. Iqbal. Vibratory stress relief in D-406 aerospace alloy. In: *TMS Annual Meeting*, pages 807–814, San Francisco, CA, USA, 2009.
- [9] J-S. Wang, C-C. Hsieh, C-M. Lin, C-W. Kuo, and W. Wu. Texture evolution and residual stress relaxation in a cold-rolled Al-Mg-Si-Cu alloy using vibratory stress relief technique. *Metallurgical and Materials Transactions A*, 44(2):806–818, 2013. doi: [10.1007/s11661-012-1450-8](https://doi.org/10.1007/s11661-012-1450-8).
- [10] W. He, B.P. Gu, J.Y. Zheng, and R.J. Shen. Research on high-frequency vibratory stress relief of small Cr12MoV quenched specimens. *Applied Mechanics and Materials*, 157-158:1157–1161, 2012. doi: [10.4028/www.scientific.net/AMM.157-158.1157](https://doi.org/10.4028/www.scientific.net/AMM.157-158.1157).
- [11] J-S. Wang, C-W. Kuo, C-C. Hsieh, H-C. Liao, and W. Wu. The effects of waveform in residual stress relief by vibration technique. In: *Trends in Welding Research 2012: Proceedings of the 9th International Conference*, pages 427–431, Chicago, IL, USA, 4–8 June, 2012.
- [12] C. Lin, S. Wu, S. Lü, P. An, and L. Wan. Effects of ultrasonic vibration and manganese on microstructure and mechanical properties of hypereutectic Al–Si alloys with 2% Fe. *Intermetallics*, 32:176–183, 2013. doi: [10.1016/j.intermet.2012.09.001](https://doi.org/10.1016/j.intermet.2012.09.001).
- [13] T. Jia, Z. Zhang, C. Tang, and Y. Zhang. Numerical simulation of stress-relief effects of protective layer extraction. *Archives of Mining Sciences*, 58(2):521–540, 2013. doi: [10.2478/amsc-2013-0035](https://doi.org/10.2478/amsc-2013-0035).
- [14] Y. Yang. Understanding of vibration stress relief with computation modeling. *Journal of Materials Engineering and Performance*, 18(7):856–86, 2009. doi: [10.1007/s11665-008-9310-9](https://doi.org/10.1007/s11665-008-9310-9).
- [15] S. Kwofie. Plasticity model for simulation, description and evaluation of vibratory stress relief. *Materials Science and Engineering: A*, 516(1-2):154–161, 2009. doi: [10.1016/j.msea.2009.03.014](https://doi.org/10.1016/j.msea.2009.03.014).
- [16] S. Aoki, T. Nishimura, T. Hiroi, and S. Hirai. Reduction method for residual stress of welded joint using harmonic vibrational load. *Nuclear Engineering and Design*, 237(2):206–212, 2007. doi: [10.1016/j.nucengdes.2006.06.004](https://doi.org/10.1016/j.nucengdes.2006.06.004).
- [17] D. Rao, D. Wang, L. Chen, and C. Ni. The effectiveness evaluation of 314L stainless steel vibratory stress relief by dynamic stress. *International Journal of Fatigue*, 29(1):192–196, 2007. doi: [10.1016/j.ijfatigue.2006.02.047](https://doi.org/10.1016/j.ijfatigue.2006.02.047).
- [18] H. Wang and Z. Wang. The embedded VSR system design based on ARM and frequency spectrum analysis. In: *2008 IEEE Pacific-Asia Workshop on Computational Intelligence and Industrial Application*, pages 488–492, Wuhan, China, 19–20 Dec., 2008. doi: [10.1109/PACIIA.2008.81](https://doi.org/10.1109/PACIIA.2008.81).
- [19] M.J. Vardanjani, M. Ghayour, and R.M. Homami. Analysis of the vibrational stress relief for reducing the residual stresses caused by machining. *Experimental Techniques*, 40(2):705–713, 2016. doi: [10.1007/s40799-016-0071-3](https://doi.org/10.1007/s40799-016-0071-3).

-
- [20] M.J. Vardanjani, A. Araee, J. Senkara, J. Jakubowski, and J. Godek. Metallurgical effects of shunting current on resistance spot-welded joints of AA2219 sheets. *Journal of Materials Engineering and Performance*, 25(8):3506–3517, 2016. doi: [10.1007/s11665-016-2168-3](https://doi.org/10.1007/s11665-016-2168-3).
- [21] M.J. Vardanjani, A. Araee, J. Senkara, M. Sohrabian, and R. Zarandooz. Influence of shunting current on the metallurgical and mechanical behaviour of resistance spot-welded joints in AA2219 joints. *Strojniški vestnik – Journal of Mechanical Engineering*, 62(11):625–635, 2016. doi: [10.5545/sv-jme.2016.3682](https://doi.org/10.5545/sv-jme.2016.3682).
- [22] B. Kılıç and Ö. Özdemir. Vibration and stability analyses of functionally graded beams. *Archive of Mechanical Engineering*, 68(1):93–113, 2021. doi: [10.24425/ame.2021.137043](https://doi.org/10.24425/ame.2021.137043).
- [23] P. Vergeer. Vibration isolation of dimple plate heat exchangers. M.Sc. Thesis. North-West University, Potchefstroom Campus, North-West University, South Africa, 2013.
- [24] S. Li, Y. Kang, G. Zhu, and S. Kuang. Effects of strain rates on mechanical properties and fracture mechanism of DP780 dual phase steel. *Journal of Materials Engineering and Performance*, 24(6):2426–2434, 2015. doi: [10.1007/s11665-015-1495-0](https://doi.org/10.1007/s11665-015-1495-0).
- [25] A. Grudz. Reducing welding stresses in plates by vibration. *Automatic Welding USSR*, 25(7):70–71, 1972.
- [26] A.S.M.Y. Munsif, A.J. Waddell, and C.A. Walker. Modification of welding stresses by flexural vibration during welding. *Science and Technology of Welding and Joining*, 6(3):133–138, 2001. doi: [10.1179/136217101101538668](https://doi.org/10.1179/136217101101538668).